PASJ: Publ. Astron. Soc. Japan **51**, 321–331 (1999)

X-Ray Evidence of an AGN in M82

Hironori MATSUMOTO*
The Institute of Physical and Chemical Research (RIKEN), 2-1 Hirosawa, Wako, Saitama 351-0198
and
Takeshi Go TSURU
Department of Physics, Faculty of Science, Kyoto University, Sakyo-ku, Kyoto 606-8502
E-mail (TGT): tsuru@cr.scphys.kyoto-u.ac.jp

(Received 1999 January 27; accepted 1999 March 24)

Abstract

The X-ray spectrum of the famous starburst galaxy M82 consists of three components: soft, medium, and hard (Tsuru et al. 1997, AAA 68.157.702). The spectrum of the hard component, which is spatially unresolved, is well represented by an absorbed thermal bremsstrahlung, or an absorbed power-law model. However, the origin of the hard component is unclear. Thus, we conducted a monitoring observation with ASCA in 1996. Although the X-ray flux of the soft and medium components remained constant, a significant time variability of the hard component was found between 3×10^{40} erg s^{-1} and 1×10^{41} erg s^{-1} at various time scales from 10 ks to one month. The temperature or photon index of the hard component also changed. We proved that the spatial position of the hard component is the center of M82. The spectrum of the variable source obtained by subtracting the spectrum of the lowest state from the highest state suggests strong absorption of $N_{\rm H} \sim 10^{22}$ cm^2, which means a variable source is embedded in the center of M82. All of these observations suggest that a low-luminosity AGN exists in M82.

Key words: Galaxies: active — Galaxies: individual (M82) — Galaxies: X-rays — X-Rays: spectra

1. Introduction

Because M82 is thought to be an archetypical starburst galaxy, many X-ray observations of M82 have been made. The first observation by ASCA of M82 was conducted in 1993. Tsuru et al. (1997) analyzed the ASCA spectrum, and found that it consists of three components: soft, medium, and hard. The soft and medium components, showing emission lines from various elements, are of thermal origin at temperatures of ~ 0.3 and ~ 1 keV. The ASCA images of the soft and medium components are extended compared with the ASCA point spread function (PSF). Thus, their origin would be the galactic wind driven by stellar winds from massive stars and supernovae.

The hard component can be well described by either a power-law model (the photon index is $\Gamma \sim 1.7$) or a thermal-plasma model (the temperature is $kT \sim 14$ keV). This component is dominant in the X-ray spectra above the 2 keV band, and its X-ray luminosity in the 2–10 keV band is $\sim 3 \times 10^{40}$ erg s^{-1}. Tsuru et al. (1997) compared the ASCA flux in the 2–10 keV band with that of Ginga (Tsuru 1992) and EXOSAT (Schaaf et al. 1989), and found a time variability. Furthermore, the spatial extent of the hard component is consistent with a point source within the ASCA angular resolution. All of these observations may suggest that the origin of the hard component is a low-luminosity AGN of M82. However, since Ginga and EXOSAT are non-imaging detectors, possible contamination from other hard sources is not excluded. Therefore, it is unclear whether the flux change can be attributed to the hard component or not. Since the peak position of the hard component does not agree with the soft component, it is unclear whether the peak of the hard component agrees with the center of M82 where a luminous X-ray point source showing time variability exists (Watson et al. 1984; Collura et al. 1994; Bregman et al. 1995; Strickland et al. 1997). Furthermore, the Ginga spectrum can be fitted with a thermal model, but cannot be fitted with a power-law model (Tsuru 1992), which is different from the typical X-ray spectra of AGNs. The same conclusion was suggested by Cappi et al. (1998) using the BeppoSAX data. Thus, the origin of the hard component is still debatable.

The first key to reveal the origin of the hard component is to clarify whether it shows a time variability or not. The second key is to detect the iron K-line emission and to determine its central energy. The central energy of the line can be direct evidence. For these purposes, we made a monitoring observation of M82 with ASCA in

* Present address: Center for Space Research, Massachusetts Institute of Technology, NE80-6045, 77 Massachusettes Avenue, Cambridge, MA 02139-4307, USA.

Table 1. Log of the observations.

Sequence	Date		Exposure			
	UT (yyyy/mm/dd)	MJD	SIS 0 (s)	SIS 1 (s)	GIS 2 (s)	GIS 3 (s)
PV	1993/04/19	49096.5	16254	16521	26694	26646
74049000	1996/03/22	50164.5	13565	13565	12932	12924
74049010	1996/04/15	50188.5	6930	6930	8668	8668
74049020	1996/04/21	50194.5	12395	12343	13140	13138
74049030	1996/04/24	50197.5	29800	29902	33294	33288
74049050	1996/05/13	50216.5	8160	8088	9688	9688
74049060	1996/05/16	50219.5	11545	11583	14386	14390
74049070	1996/10/14	50370.5	8941	8941	7612	7612
74049080	1996/11/14	50401.5	12033	12103	12498	12496
74049090	1996/11/26	50413.5	8762	8730	9792	9760

1996. The total exposure time, including the observation in 1993, is about 1.5×10^5 s.

Throughout this paper, a distance of 3.25 Mpc to M82 is assumed. The number of atoms per hydrogen for the cosmic metal abundance adopted in this paper are 9.77×10^{-2} for He, 3.63×10^{-4} for C, 1.12×10^{-4} for N, 8.51×10^{-4} for O, 1.23×10^{-4} for Ne, 3.80×10^{-5} for Mg, 3.55×10^{-5} for Si, 1.62×10^{-5} for S, 3.63×10^{-6} for Ar, 2.29×10^{-6} for Ca, 4.68×10^{-5} for Fe, and 1.78×10^{-6} for Ni (Anders, Grevesse 1989).

2. Observation and Data Reduction

ASCA observed M82 once in 1993, and observed it nine times in 1996. Though the results of the observation in 1993 have been reported by many authors (Tsuru et al. 1994; Awaki et al. 1996; Tsuru et al. 1996; Moran, Lehnert 1997; Ptak et al. 1997; Tsuru et al. 1997; Dahlem et al. 1998), we reanalyzed the data in 1993 using the same method as for the 1996 data to systematically investigate the time variability of M82. The dates of these observations are listed in table 1.

All of the data were obtained with two solid-state imaging spectrometers (SIS 0 and SIS 1) and two gas-imaging spectrometers (GIS 2 and GIS 3) at the foci of four thin-foil X-ray mirrors (XRT) on board the ASCA satellite. Details concerning the instruments can be found in Burke et al. (1991), Ohashi et al. (1996), Makishima et al. (1996), and Serlemitsos et al. (1995), while Tanaka et al. (1994) give a general description of ASCA. The SIS data were obtained in the 4-CCD bright mode for the observation in 1993 and in the 1-CCD faint mode for the other observations in 1996. The GIS data were obtained in the normal PH mode.

All of the data were screened with the standard selection criteria: data taken in the South Atlantic Anomaly, Earth occultation, and regions of low geomagnetic rigidity are excluded. We also eliminated the contamination by the bright Earth, removed hot and flickering pixels from the SIS data, and applied rise-time rejection to exclude particle events from the GIS data. We further applied the "flare-cut" criteria to exclude as many non X-ray background events as possible for the GIS data (Ishisaki et al. 1997, ASCA News No. 5, p26). After these screenings, we obtained effective exposure times given in table 1.

3. Analysis and Results

3.1. Imaging Analysis

Following Tsuru et al. (1997), we made SIS images (SIS 0 + SIS 1) in three energy bands (0.4–0.8 keV, 1.2–1.8 keV, and 3.0–10 keV) for an individual observation. We call them the soft-, medium-, and hard-band images, respectively. The three energy bands represent the three spectral components found by Tsuru et al. (1997). Though the soft-band images show somewhat complex structures, we found that all of the medium- and hard-band images are single-peaked and no other significant source exists in the field-of-view.

Tsuru et al. (1997) found from the PV data (1993 April 19) that the radial profiles of the soft- and medium-band images are extended compared with the ASCA PSF, while the hard-band image is consistent with a point source. They also found that the peak position of the hard-band image agrees with that of the medium-band image, but does not agree with that of the soft-band image. We confirmed these results of Tsuru et al. (1997) for all the ASCA data in 1996. For example, we show the SIS images of #74049000 (1996 March 22) in figure 1. The soft-band peak is at $\sim 0'.6$ southeast of the hard- and medium-band peaks.

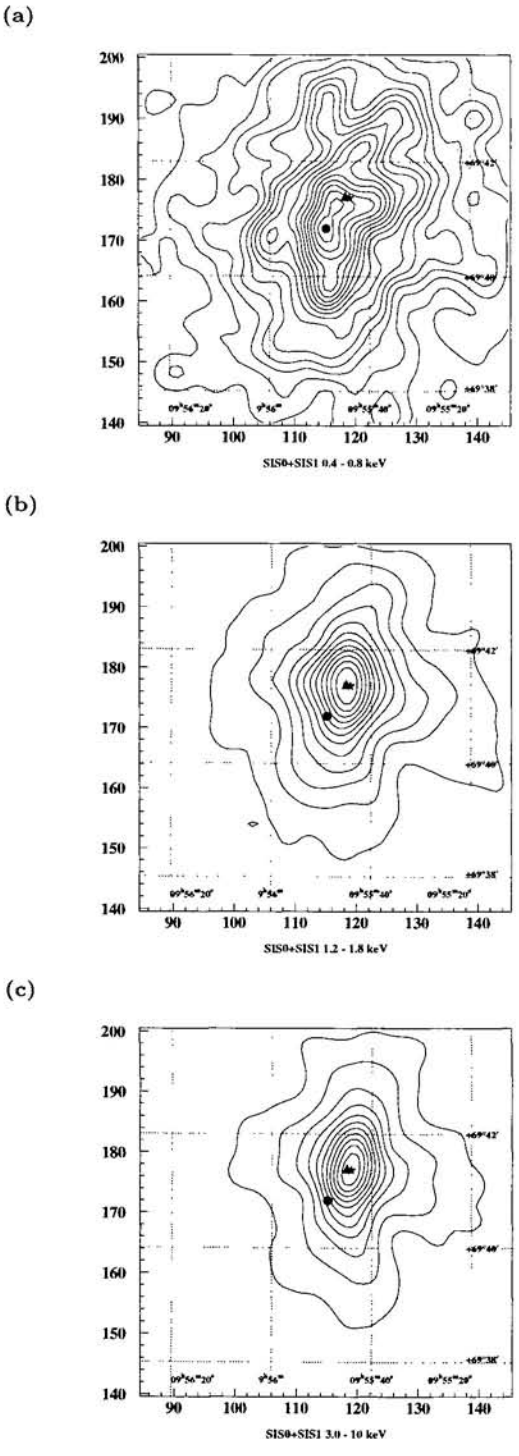

Fig. 1. SIS images of M82 from #74049000 (1996 March 22) without background subtraction and vignetting correction, (a) in the 0.4–0.8 keV band, (b) in the 1.2–1.8 keV band, and (c) in the 3.0–10 keV band. The pixel size is 6.″4, and the images were smoothed with a Gaussian distribution of $\sigma = 2$ pixel. The contour levels are 0.1, 0.2, 0.3, ... c/pixel for (a), and 1, 2, 3,... c/pixel for both (b) and (c). Dots, triangles, and stars denote the peaks of the soft-, medium-, and hard-band images, respectively.

The 90% confidence level error circle of the pointing position of ASCA is $\sim 1.'3$ diameter (Gotthelf 1996, ASCA News No. 4, p31). Except for #74049090 (1996 November 26), the peak positions of hard-band images are consistent among observations within $\sim 0.'8$. The hard-band peak of #74049090 is located at $\sim 1.'4$ southeast of that of the PV data (1993 April 19), which is still almost at the edge of the error circle. Thus, we conclude that the hard-band peaks were located at the same position within the error, and hence the source at the hard-band peak is identical through all the observations. The position of the hard-band peak determined from the ASCA SIS data is $(\alpha, \delta)_{\rm J2000} = (9^{\rm h}55^{\rm m}52^{\rm s},\ 69°40'48'')$.

3.2. *Light Curve*

From the screened data, we extracted the GIS and SIS light curves for each observation from circular regions centered on M82 in two energy bands (0.7–1.5 keV and 3.0–10.0 keV). The bin width of the light curves is 128 s. The extraction radii are $6'$ for the GIS and $4'$ for the SIS, which are nominal for a bright point source according to "The ASCA DATA Reduction Guide" presented by the ASCA Guest Observer Facility (http://heasarc.gsfc.nasa.gov/docs/asca/abc/abc.html). Next, we combined the light curves of the SIS 0 and SIS 1, and the GIS 2 and GIS 3.

We fitted the light curves of the GIS 2 + GIS 3 with a constant counting-rate model. In most cases, the reduced χ^2 ($= \chi^2$/d.o.f.) is less than 1.5, which means no apparent time variability. However, the reduced χ^2 is 2.7 for the GIS light curve of #74049030 (1996 April 24) in the 3.0–10.0 keV band, though we can see no clear time variability in the 0.7–1.5 keV band at that time (figure 2). The SIS data are consistent with these results of the GIS. As mentioned in the previous section, only one identical source was found in the field-of-view through all observations. Therefore, this result strongly suggests that the hard component of M82 detected by Tsuru et al. (1997) has short-term variability on a time scale of $\sim (1\text{–}2) \times 10^4$ s, while the soft component has no clear time variability.

3.3. *Spectral Analysis*

From the screened data, we extracted the SIS and GIS spectra from the same regions as those for the light curves. We then rebinned the spectra to contain at least 20 counts in each spectral bin to utilize the χ^2 technique.

We extracted the background spectra for the GIS from the blank sky data taken during the Large Sky Survey project (e.g., Ueda et al. 1998) with the same data-reduction method for the data of M82. We obtained the SIS background spectra for the PV data in 1993 from a source-free region around M82. Because the observations in 1996 were conducted with the 1-CCD faint mode and

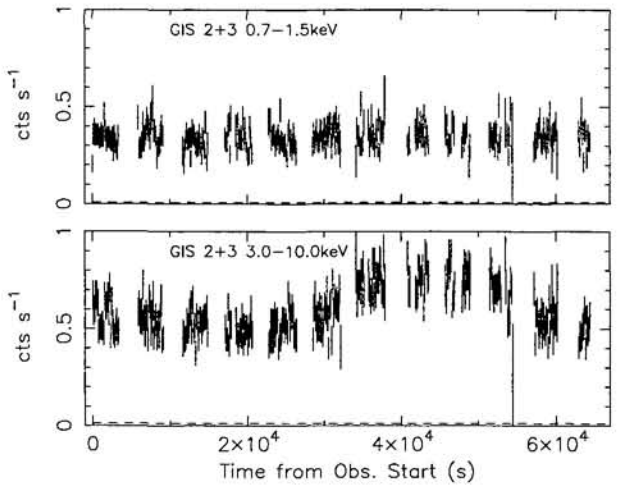

Fig. 2. Light curves of the GIS 2+3 during the observation of #74049030 (1996 April 24). Each bin width is 128 s. The horizontal axis is the time after starting the observation. No background subtraction was applied. The background levels (0.0079 c s^{-1} for the 0.7–1.5 keV band and 0.012 c s^{-1} for the 3.0–10.0 keV band) are indicated by the dashed lines.

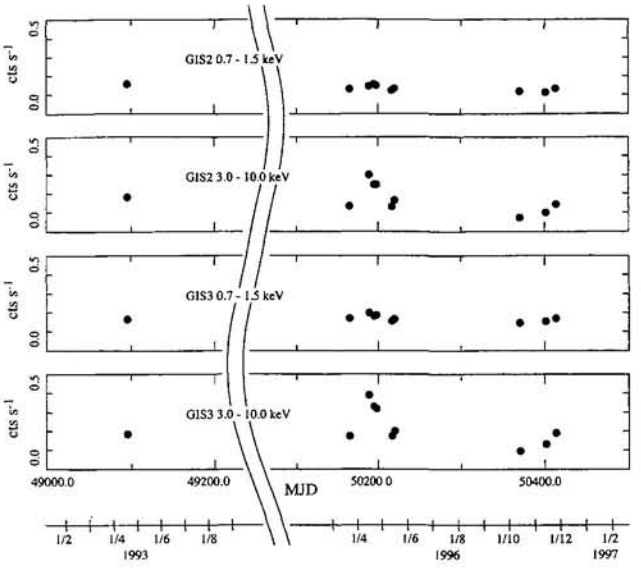

Fig. 3. Count rates of the GIS 2+3 in the 0.7–1.5 keV and 3.0–10 keV bands. The error bars are smaller than the data points.

X-rays from M82 covered the whole region of the CCD chip, we could not define the source-free regions for the observations in 1996. Therefore, to extract the background spectra, we used the data of LSS 1988 + 317, which is a dim source observed in the 1-CCD faint mode in 1996 (Sakano et al. 1998). After applying the same data reduction as that for M82, we extracted the background spectra from a source-free region.

The count rates of the spectra in the 0.7–1.5 keV and 3.0–10 keV bands are shown in figure 3. They are background subtracted, but not vignetting corrected values. The count rates in the 3–10 keV band show a rather large time variability compared with those in the 0.7–1.5 keV band. This suggests that the hard component (Tsuru et al. 1997) has long-term variability on a time scale of $\sim$ one month. Because the detector positions of M82 were almost the same for all observations in 1996, the vignetting correction does not change the results essentially.

3.3.1. Time variability of the hard component

First, we fitted the SIS 0 and SIS 1 spectra in the 0.6–10 keV band and the GIS 2 and GIS 3 spectra in the 0.7–10 keV band simultaneously with the three-temperature thermal plasma model applied in Tsuru et al. (1997). The model can be represented by

$$N_{\rm H}({\rm whole}) \times [{\rm RS(soft)} + N_{\rm H}({\rm medium}) \times {\rm RS(medium)} + N_{\rm H}({\rm hard}) \times {\rm RS(hard)}], \quad (1)$$

where $N_{\rm H}$ is the equivalent hydrogen column density of an absorbing cold material and RS is the thin thermal plasma model developed by Raymond and Smith (1977) (hereafter RS model). The soft and medium components are assumed to have the same metal abundance, and the abundance ratios among metals of the hard component are fixed to be cosmic. The column densities, temperatures, and metal abundances of the soft and medium components are fixed to the best-fit values of Tsuru et al. (1997); $N_{\rm H(whole)} = 3.0 \times 10^{20}$ cm^{-2}, $N_{\rm H(medium)} = 0.0$ cm^{-2}, kT(soft) = 0.32 keV, kT(medium) = 0.95 keV, He = C = 1.0 cosmic, N = 0.0 cosmic, O = 0.063 cosmic abimdamce, Ne = 0.15 cosmic, Mg = 0.25 cosmic, Si = 0.40 cosmic, S = 0.47 cosmic, Ar = Ca = 0.0 cosmic, and Fe = Ni = 0.049 cosmic. Thus, the free parameters are the column density, temperature, metal abundance, normalization of the hard component, and the normalizations of the soft and medium components. This 3RS model could fit all the spectra quite well. The best-fit parameters are given in table 2. The luminosities of the soft and medium components are quite stable, while the hard component has a clear time variability. This is shown in figure 4.

The hard component could also be fitted with a power-law model (Tsuru et al. 1997). Therefore, we also tried the 2RS + power-law model, which is expressed as

$$N_{\rm H}({\rm whole}) \times [{\rm RS(soft)} + N_{\rm H}({\rm medium}) \times {\rm RS(medium)} + N_{\rm H}({\rm hard}) \times {\rm Power\text{-}law(hard)}]. \quad (2)$$

Table 2. Results of the 3RS model fitting.*

Sequence	$N_{\rm H}$	kT	Abundance	$F_{\rm X}^{\dagger}(10^{-11}$ erg s^{-1} cm$^{-2})$			$L_{\rm X}^{\ddagger}(10^{40}$ erg s$^{-1})$			χ^2/d.o.f.
	10^{22} cm^{-2}	keV	cosmic	soft	medium	hard§	soft	medium	hard§	
PV	$2.20^{+0.34}_{-0.33}$	$11.2^{+2.0}_{-1.6}$	$0.18^{+0.08}_{-0.06}$	0.44	0.70	2.0 (1.9)	1.8	1.6	4.2 (2.9)	1053.6/1022
74049000	$1.89^{+0.31}_{-0.29}$	$4.47^{+0.41}_{-0.38}$	$0.036^{+0.042}_{-0.036}$	0.34	0.88	2.2 (2.1)	1.4	2.0	5.6 (3.2)	796.2/840
74049010	$1.35^{+0.25}_{-0.23}$	$10.2^{+1.5}_{-1.3}$	$0.026^{+0.071}_{-0.026}$	0.41	0.76	5.5 (5.2)	1.6	1.7	11 (7.4)	859.1/870
74049020	$1.38^{+0.19}_{-0.18}$	$8.17^{+0.81}_{-0.73}$	$0.033^{+0.044}_{-0.033}$	0.43	0.73	4.5 (4.2)	1.7	1.7	9.1 (6.1)	1097.7/1065
74049030	$1.47^{+0.13}_{-0.13}$	$7.40^{+0.41}_{-0.38}$	$0.036^{+0.026}_{-0.027}$	0.42	0.74	4.4 (4.1)	1.7	1.7	9.2 (6.0)	1739.1/1594
74049050	$1.74^{+0.56}_{-0.54}$	$16.0^{+7.0}_{-4.6}$	$0.00^{+0.14}_{...}$	0.34	0.82	2.3 (2.2)	1.4	1.9	4.4 (3.2)	634.0/596
74049060	$1.58^{+0.30}_{-0.28}$	$8.08^{+1.14}_{-0.90}$	$0.075^{+0.060}_{-0.063}$	0.34	0.85	2.8 (2.6)	1.4	1.9	5.8 (3.9)	929.9/889
74049070	$3.66^{+0.99}_{-0.91}$	$5.70^{+2.20}_{-1.32}$	$0.22^{+0.13}_{-0.12}$	0.33	0.82	1.2 (1.1)	1.3	1.9	3.1 (2.0)	338.1/315
74049080	$2.84^{+0.73}_{-0.72}$	$11.7^{+6.8}_{-3.2}$	$0.12^{+0.13}_{-0.12}$	0.36	0.77	1.7 (1.7)	1.5	1.8	3.7 (2.6)	544.7/479
74049090	$1.76^{+0.75}_{-0.79}$	$11.9^{+5.7}_{-3.1}$	$0.090^{+0.13}_{-0.090}$	0.37	0.80	2.6 (2.5)	1.5	1.8	5.1 (3.6)	490.9/466

*All the errors are described at 90% confidence limits.
†Flux in the 0.5–10 keV band.
‡Unabsorbed luminosity in the 0.5–10 keV band.
§Values in parentheses are in the 2–10 keV band.

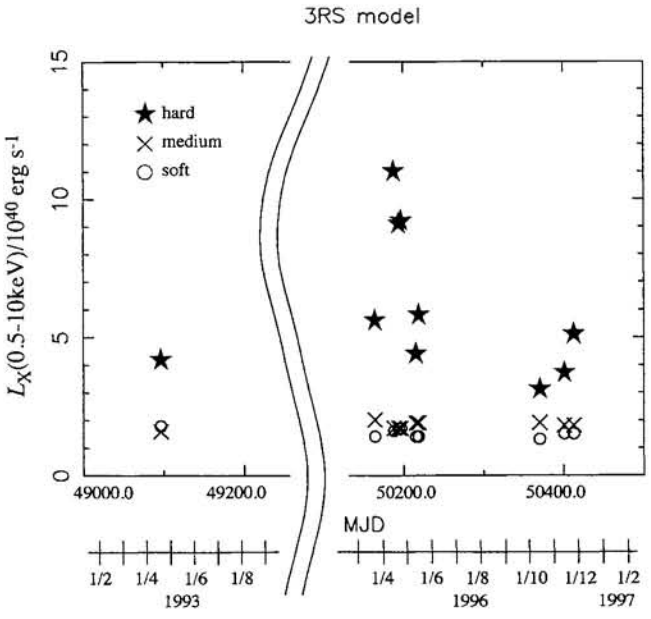

Fig. 4. Time variability of each component in the 3RS model. The stars, crosses, and circles show the hard, medium, and soft components, respectively.

The soft and medium components are assumed to have the same metal abundances. The column densities, temperatures, and metal abundance of the soft and medium components were fixed to the best-fit values of Tsuru et al. (1997); $N_{\rm H(whole)} = 3.0 \times 10^{20}$ cm^{-2}, $N_{\rm H(medium)} = 0.0$, kT(soft) = 0.31 keV, kT(medium) = 0.95 keV, He = C = 1.0 cosmic abundance, N = 0.0 cosmic, O = 0.061 cosmic, Ne = 0.14 cosmic, Mg = 0.25 cosmic, Si = 0.40 cosmic, S = 0.45 cosmic, Ar = Ca = 0.0 cosmic, and Fe = Ni = 0.048 cosmic. Thus, the free parameters were the column density, photon index, normalization of the hard component, and the normalization of the soft and medium components. This 2RS + power-law model could also fit all of the GIS and SIS spectra. The best-fit parameters are given in table 3. Only the hard component shows a time variability, which is the same as the results of the 3RS model fitting. Though both the 3RS and 2RS + power-law models could fit the spectra well, we should note that the χ^2 values of the 3RS model are generally smaller than those of the 2RS + power-law model.

Figure 5 shows the GIS 2 spectra of the highest state (#74049010; 1996 April 15) and the lowest state (#74049070; 1996 October 14). This figure also shows that only the hard component has a significant time variability. Therefore, we could obtain the spectrum of the variable component by subtracting the spectrum of the lowest state from the highest state, which is shown in figure 6. The spectrum could be fitted by either the heavily absorbed RS or heavily absorbed power-law model (table 4).

Table 3. Results of the 2RS + power-law model fitting.*

Sequence	N_H	Photon Index	$F_X^\dagger(10^{-11}$ erg s^{-1} cm$^{-2})$			$L_X^\ddagger(10^{40}$ erg s$^{-1})$			χ^2/d.o.f.
	10^{22} cm^{-2}		soft	medium	hard§	soft	medium	hard§	
PV	$2.87^{+0.41}_{-0.40}$	$1.79^{+0.08}_{-0.08}$	0.42	0.75	2.0 (1.9)	1.7	1.7	5.1 (3.1)	1080.4/1023
74049000	$3.07^{+0.40}_{-0.37}$	$2.51^{+0.11}_{-0.10}$	0.30	0.98	2.2 (2.1)	1.3	2.2	11 (3.7)	817.2/841
74049010	$1.90^{+0.31}_{-0.29}$	$1.83^{+0.08}_{-0.07}$	0.37	0.88	5.5 (5.2)	1.5	2.0	13 (7.9)	876.9/871
74049020	$2.00^{+0.24}_{-0.23}$	$1.96^{+0.06}_{-0.06}$	0.40	0.84	4.5 (4.2)	1.6	1.9	12 (6.5)	1121.2/1066
74049030	$2.25^{+0.17}_{-0.17}$	$2.04^{+0.04}_{-0.04}$	0.37	0.89	4.4 (4.1)	1.5	2.0	12 (6.5)	1832.8/1595
74049050	$2.35^{+0.70}_{-0.64}$	$1.69^{+0.14}_{-0.13}$	0.32	0.87	2.3 (2.2)	1.3	2.0	5.1 (3.3)	637.1/597
74049060	$2.23^{+0.38}_{-0.34}$	$1.96^{+0.08}_{-0.09}$	0.31	0.92	2.8 (2.7)	1.3	2.1	7.5 (4.1)	949.6/890
74049070	$4.27^{+1.17}_{-1.06}$	$2.10^{+0.26}_{-0.24}$	0.32	0.83	1.2 (1.2)	1.3	1.9	4.3 (2.1)	347.5/316
74049080	$3.65^{+0.85}_{-0.83}$	$1.80^{+0.18}_{-0.16}$	0.34	0.81	1.7 (1.7)	1.4	1.8	4.6 (2.8)	549.5/480
74049090	$2.75^{+0.77}_{-0.79}$	$1.82^{+0.16}_{-0.15}$	0.32	0.90	2.6 (2.5)	1.3	2.1	6.5 (3.9)	501.2/467

*All the errors are described at 90% confidence limits.
†Flux in the 0.5–10 keV band.
‡Unabsorbed luminosity in the 0.5–10 keV band.
§Values in parentheses are in the 2–10 keV band.

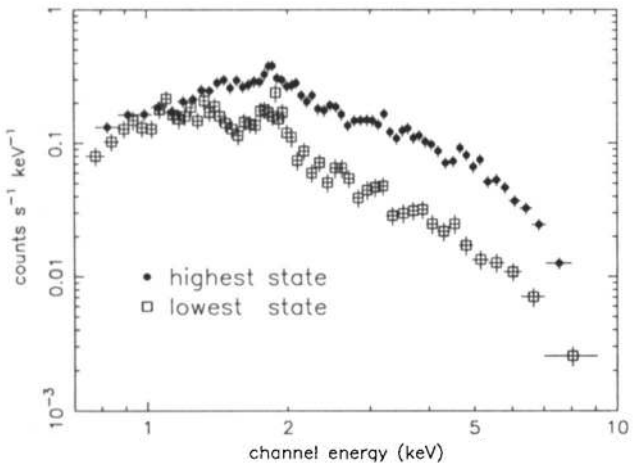

Fig. 5. GIS 2 spectra of the highest state (#74049010; 1996 April 15) and the lowest state (#74049070; 1996 October 14).

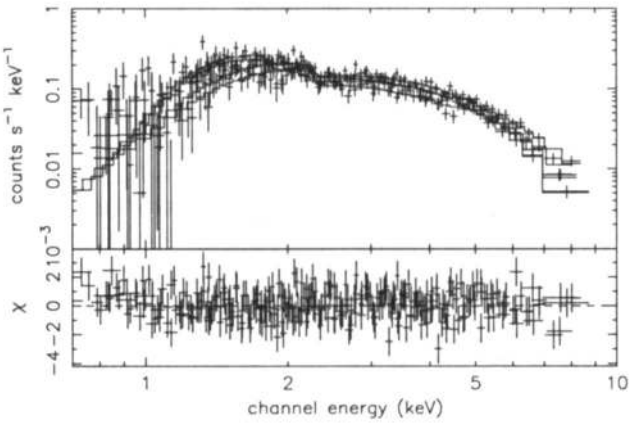

Fig. 6. Residual spectra of the SIS 0, SIS 1, GIS 2, and GIS 3 obtained by subtracting the lowest state (#74049070; 1996 April 15) from the highest state (#74049010; 1996 October 14). The lines show the best-fit heavily absorbed RS model.

3.3.2. Iron K-line emission

Information concerning the iron K-line emission is one of the essential keys to determine the origin of the hard component. Since the statistics of an individual observation are limited, we added all of the GIS spectra. Since the PV data in 1993 obtained in the 4-CCD bright mode in 1993 are thought to be quite different in quality from those obtained in the 1-CCD faint mode in 1996, we added only the data in 1996 for the SIS. Before adding the spectra, we confirmed the accuracy of the gain calibration using the center energy of the silicon K line at 1.86 keV. We then simultaneously analyzed the added SIS and GIS spectra and the SIS spectra in 1993 above the 4 keV band.

Table 4. The results of the fitting of the residual spectra.*

	RS	Power-law
N_H (10^{22} cm^{-2})	$1.30^{+0.12}_{-0.10}$	$1.54^{+0.16}_{-0.14}$
Temperature (keV)	$11.7^{+2.6}_{-2.1}$	...
Abundance (cosmic)	$0.00^{+0.088}$	...
Photon index	...	$1.72^{+0.09}_{-0.08}$
Flux (0.5–10 keV) (erg s^{-1} cm^{-2})	4.5×10^{-11}	4.6×10^{-11}
Flux (2–10 keV) (erg s^{-1} cm^{-2})	4.2×10^{-11}	4.3×10^{-11}
Luminosity (0.5–10 keV) (erg s^{-1})	8.3×10^{40}	9.5×10^{-11}
Luminosity (2–10 keV) (erg s^{-1})	5.8×10^{40}	6.1×10^{-11}
χ^2/d.o.f.	272.0/274	279.5/275

*All the errors are described at 90% confidence limits.

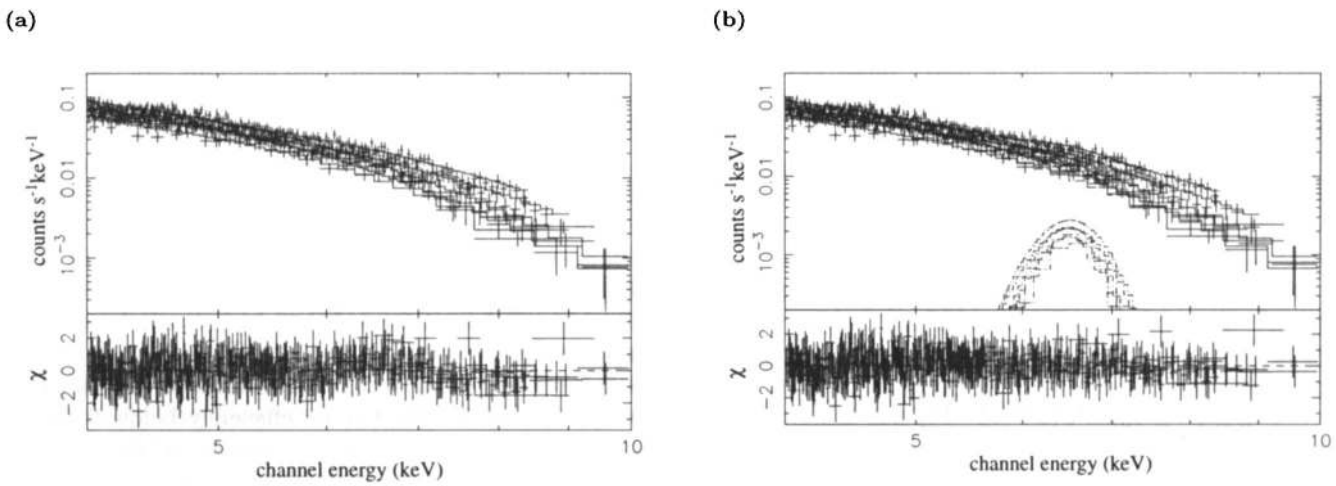

Fig. 7. Composite SIS and GIS spectra and the SIS spectra in 1993 above the 4 keV band. The solid lines show the best-fitting models: (a) thermal bremsstrahlung model, and (b) thermal bremsstrahlung + Gaussian line model.

First, we fitted the spectra with a thermal bremsstrahlung model. The quality of the fit is good (χ^2/d.o.f. = 350.4/563), and is shown in figure 7a and table 5. Next, we added a Gaussian line model to the thermal bremsstrahlung (Brems. +1 Gaussian). The result is given in figures 7b, 8, and table 5, and the χ^2/d.o.f. is 330.8/560. The decrease of the χ^2 value is 19.6, while the decrease of the d.o.f. is 3. Therefore, we can conclude that ASCA detected the iron K line with a significant line width of $\sigma \sim 0.3$ keV at a significance level of more than 99.5% (Malina et al. 1976).

Assuming line broadening of 0.3 keV, the results from the outflow motion of the hot gas, the velocity of the gas should be 1.4×10^9cm s^{-1}, which is too much higher than that estimated (e.g., McKeith et al. 1995). The detected line center energy is between the iron 6.4 keV and 6.7 keV. Thus, the obtained broad line suggests a superposition of a few lines, as seen in our galactic center (Koyama et al. 1996). Therefore, we added two narrow Gaussian lines ($\sigma = 0$) to the bremsstrahlung model (Brems. +2 Gaussians). The best-fit parameters are given in table 5. In this case, the two lines can be attributed to the iron 6.4 keV and 6.7 keV lines. Finally, we tried three narrow Gaussian lines plus the bremsstrahlung model in which the center energy is fixed to 6.4 keV, 6.7 keV, and 7.0 keV (Brems. +3 Gaussians). The results are also given in table 5.

Table 5. The best-fit parameters of the model fitting to the spectra above the 4 keV band.*

	Brems.	Brems. + 1 Gaussian	Brems.+ 2 Gaussians		Brems. + 3 Gaussians		
Temperature	$12.56^{+1.95}_{-1.33}$	$10.19^{+1.84}_{-1.05}$	$10.71^{+1.43}_{-1.14}$		$10.51^{+1.48}_{-1.16}$		
Center energy (keV) ...	...	$6.56^{+0.14}_{-0.14}$	$6.34^{+0.12}_{-0.14}$	$6.68^{+0.17}_{-0.11}$	6.4†	6.7†	7.0†
Line width (σ) (keV) ..	...	$0.30^{+0.16}_{-0.19}$	0†	0†	0†	0†	0†
Equivalent width (eV) .	...	121^{+58}_{-61}	39^{+26}_{-25}	52^{+31}_{-30}	45^{+26}_{-25}	39^{+31}_{-31}	22^{+37}_{-22}
χ^2/d.o.f.	350.4/563	330.8/560	330.2/559		330.0/560		

*All the errors are described at 90% confidence limits.
†Fixed.

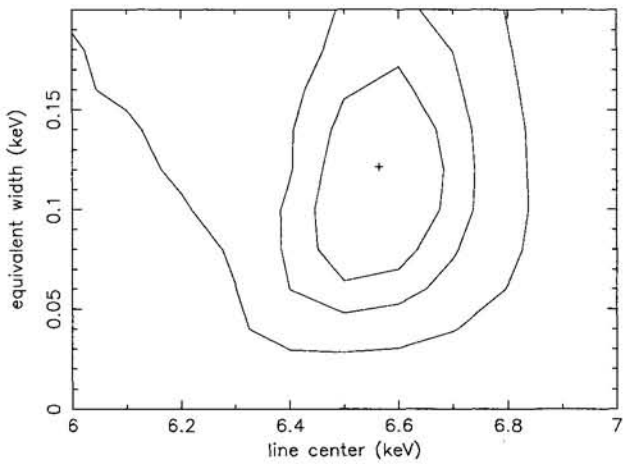

Fig. 8. Confidence contours at $\Delta\chi^2 = 2.3$, 4.61, and 9.21 for the line center energy and equivalent width of the iron K line.

4. Discussion

4.1. Identification of the Hard Component

Two bright X-ray sources showing time variability have been detected with the Einstein HRI and ROSAT HRI (Watson et al. 1984; Collura et al. 1994); sources 1 and 2 of Collura et al. (1994). We call them source 1 and source 2, hereafter. The position of the hard component determined solely from the ASCA SIS data is $(9^h55^m52^s, 69°40'48'')_{J2000}$ with an error circle of $\sim 40''$ radius in 90% confidence level (Gotthelf 1996, ASCA News No. 4, p31). The error circle includes source 2. However, the position of the hard component does not agree with source 1, whose position is outside the error circle.

Next, we determine the precise position of the hard component by comparing the ASCA SIS image with the ROSAT HRI image. Making the ASCA SIS image in the same energy range as the ROSAT HRI and comparing it with the actual ROSAT HRI image is insufficient, because the shape of effective area as a function of X-ray energy is different between the two instruments. Therefore, we make a fake ROSAT HRI image from the ASCA SIS data by taking the energy dependence of the effective area of the two instruments into account, and comparing it with the actual ROSAT HRI image.

To fake the HRI image, we first made four SIS images in the 0.4–0.8 keV, 0.8–1.2 keV, 1.2–1.6 keV, and 1.6–2.0 keV bands. Next, we multiplied each image by the ratio of the effective area of the HRI to that of the SIS in each energy band. For the effective area of the ROSAT HRI, we used the values in Briel et al. (1996). For the SIS image of the 0.4–0.8 keV band, particularly, we multiplied it by the ratio of the effective area of the HRI in the 0.1–0.8 keV band to that of the SIS in the 0.4–0.8 keV band, because the SIS has no efficiency below 0.4 keV. Finally, we made a fake HRI image by adding all four images. In figure 9, we show the fake HRI image using the data of #74049000 (1996 March 22) as an example. From this analysis, we found that the peak position of the fake HRI image agrees with the ASCA hard-band peak. Please note that the fake HRI image almost reflects the ASCA medium-band image, because the peak of effective area as a function of the X-ray energy of the ROSAT HRI is at ~ 1.1 keV (Briel et al. 1996). Because the peak of the fake HRI image should be at the peak of the real HRI image, we conclude that the ASCA hard-band peak agrees with the peak of the real HRI image, which is located at the nucleus of M82 (Collura et al. 1994; Strickland et al. 1997).

Source 2 is time variable and located at the peak of the HRI image. This source is reported to correspond to a strong 6-cm radio source 41.5 + 597 (Strickland et al. 1997), which showed a 100% drop in flux within a year (Muxlow et al. 1994). We estimated the count rate of the ROSAT HRI of the hard component from the best-fit parameters given in tables 2 and 3, and compared it with source 2. When we applied the RS model

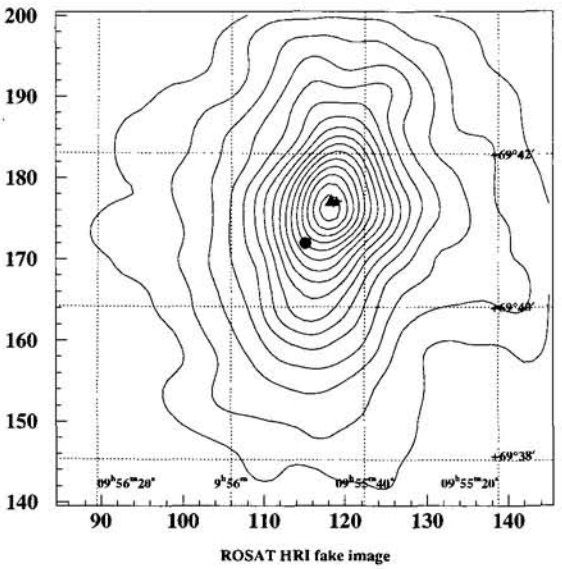

Fig. 9. Fake ROSAT HRI image made of the SIS images of #74049000 (1996 March 22) without background subtraction and vignetting correction. The pixel size is 6.″4, and the image was smoothed with a Gaussian distribution of $\sigma = 2$ pixel. The contour levels are 1, 2, 3, ... c/pixel. The symbols are the same as in figure 2.

for the hard component, the count rates of the ROSAT HRI were estimated to be 0.017 c s^{-1}, 0.096 c s^{-1}, and 0.0040 c s^{-1} for the PV data (1993 April 19), the highest state (#74049010; 1996 April 15), and the lowest state (#74049070; 1996 October 14), respectively. In the case of the power-law model, the count rates were estimated to be 0.012 c s^{-1} for the PV data, 0.075 c s^{-1} for the highest state, and 0.0040 c s^{-1} for the lowest state. The range of these estimated counting rates of the hard component includes the actual ROSAT HRI counting rates of 0.04–0.06 c s^{-1} of source 2. Thus, we conclude that the hard component at the ASCA hard-band peak is identical with source 2.

4.2. Origin of the Hard Component

The hard component has a time variability of 10^4 s–a month with a luminosity of 3×10^{40}–1×10^{41} erg s^{-1}. A collection of discrete sources such as X-ray binaries, a super-Eddington source, a young SNR, inverse Compton scattering of IR photons from relativistic electrons which produce the radio emission, hot interstellar medium, and an AGN have been considered so far as an origin of the hard X-ray emission. Since the typical X-ray luminosity of X-ray binaries is $\sim 10^{37}$ erg s^{-1}, a few hundred binaries are needed to explain the luminosity of the hard X-ray emission of M82. Therefore, a collection of binaries cannot explain the time variability of M82. Since the typical luminosity of super-Eddington sources is $\sim 10^{40}$ erg s^{-1} (Okada et al. 1998), it cannot explain the highest luminosity of M82. A young SNR cannot become as bright as M82 did in our observation. The radio emission is extended as large as $\sim 30''$ (Kronberg, Clarke 1978), which corresponds to $\sim 1.5 \times 10^{21}$ cm, while the time variability on a time scale of $\sim 1 \times 10^4$ s implies the size of the emitting region to be smaller than 3×10^{14} cm. Therefore, the inverse Compton emission cannot explain the time variability. It is also quite an unnatural situation that the hot interstellar medium with a temperature of ~ 10 keV is confined to a region smaller than 3×10^{14} cm. Therefore, an AGN is the only possible origin that can explain the luminosity and time variability.

The X-ray luminosity of the hard component is similar to that of low-luminosity AGNs (LLAGN) (Terashima et al. 1998b). We proved that the hard component is located at the center of M82 and is spatially unresolved. The residual spectrum obtained by subtracting the spectrum of the lowest state (#74049070; 1996 October 14) from the highest state (#74049010; 1996 April 15) suggests strong absorption, which means that the variable source is embedded in the galactic center region of M82. These observations also strongly support the LLAGN as being the origin of the hard component. Because the violent starburst activity dominates the AGN activity, there has been no evidence of the AGN in other wavelengths (e.g., Luts et al. 1998), and one can detect the AGN activity only in the hard X-ray band, like NGC 6240 (Iwasawa, Comastri 1998). Though we could not constrain the center energy of the iron K line, Cappi et al. (1998) determined the center energy to be 6.7 keV, which may suggest a thermal origin of the hard component. However, we should note that some of the LLAGNs have a broad iron K line at 6.7 keV, rather than at 6.4 keV (Ishisaki et al. 1996; Terashima et al. 1998a).

As mentioned above, the time variability implies the size of the emitting region to be smaller than 3×10^{14} cm. Assuming that the origin of the hard component is the LLAGN and the X-rays are mainly emitted from a region as large as 6 times its Schwarzschild radius, the mass of the central object is estimated to be less than $2 \times 10^8 M_\odot$. The temperature, photon index, and column density given in tables 2 and 3 are also not constant, though there is no clear correlation between them. However, there is a correlation between the column density and the luminosity of the hard component: the column density increases as the luminosity decreases (figure 10). The same tendency can be seen in NGC 4151, which is the only known source showing a variable column density (Yaqoob et al. 1993).

Though the most plausible origin of the hard component is a LLAGN, the spectral shape is somewhat strange. The χ^2 values of the 3RS model fitting are generally smaller than those of the 2RS + power-law model

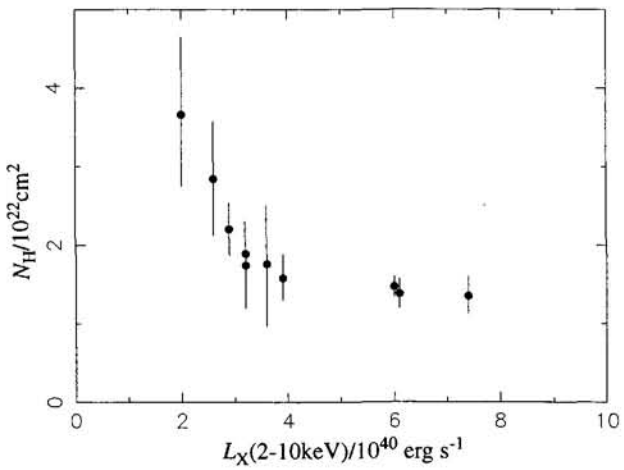

Fig. 10. Column density of the hard component plotted against the luminosity of the hard component in the 2–10 keV band. The column density and luminosity were evaluated with the 3RS model.

fitting. The Ginga spectrum could be fitted by the thermal bremsstrahlung model but could not be fitted by the power-law model (Tsuru 1992). Almost the same conclusion was reported by Cappi et al. (1998) using the BeppoSAX data. All of these observations suggest that the spectral shape is thermal-like, while the typical LLAGN shows a power-law spectrum. Therefore, it may also be possible that the origin of the hard component is a new type of accreting X-ray source.

5. Conclusion

We found a time variability of the hard component of M82 detected by Tsuru et al. (1997) on a time scale of 10^4 s–one month. The luminosity of the hard component in the 0.5–10 keV band ranges from 3×10^{40} erg s^{-1} to 1×10^{41} erg s^{-1}. The spatial position of the hard component agrees with the luminous X-ray point source at the center of M82, detected with ROSAT and Einstein observatories (Watson et al. 1984; Collura et al. 1994; Bregman et al. 1995; Strickland et al. 1997). The spatial extent of the hard component is consistent with a point source. The residual spectrum obtained by subtracting the spectrum of the lowest state from the highest state suggests a strong absorption feature, which means that the variable source is embedded in the galactic center region of M82. All of these observations strongly suggest that there is a hidden LLAGN in M82, though its spectral shape is different from that of typical LLAGNs. We also detected a broad iron K line at $6.56^{+0.14}_{-0.14}$ keV or a superposition of a few iron K lines. There is a correlation between the column density and the luminosity of the hard component. This first firm evidence of a LLAGN in M82 suggests a link between starbursts and AGN.

Note added in proof

After submitting this paper, the authors have become aware of the paper by Ptak and Griffiths (astro-ph/9903372), which obtains the similar results to this paper using the same data independently.

The authors thank K. Koyama, S. Ueno, Y. Terashima, and S. Yamauchi for helpful discussion and useful comments. They are also grateful to P. Hilton for careful review of the manuscript. HM is supported by the Special Postdoctoral Researchers Program of RIKEN. The authors also thank the ASCA team members for their support.

References

Anders E., Grevesse N. 1989, Geochim. Cosmochim. Acta 53, 197
Awaki H., Tsuru T., Koyama K. ASCA team 1996, in UV and X-Ray Spectroscopy of Astrophysical and Laboratory Plasmas, ed K. Yamashita, T. Watanabe (Universal Academy Press, Tokyo) p327
Bregman J.N., Schulman E., Tomisaka K. 1995, ApJ 439, 155
Briel U.G., Aschenbach B., Hasinger G., Hippmann H., Pfeffermann E., Predehl P., Schmitt J.H.M.M., Voges W. et al. 1996, The ROSAT User's Handbook (Max-Plank-Institut für extraterrestrische Physik, Garching D-85740, Germany)
Burke B.E., Mountain R.W., Harrison D.C., Bautz M.W., Doty J.P., Ricker G.R., Daniels P.J. 1991, IEEE Trans. ED-38, 1069
Cappi M., Persic M., Mariani S., Bassabu L., Danese L., Dean A.J., Di Cocco G., Franceschini A. et al. 1998, astro-ph/9809325
Collura A., Reale F., Schulman E., Bregman J.N. 1994, ApJ 420, L63
Dahlem M., Weaver K.A., Heckman T.M. 1998, ApJS 118, 401
Ishisaki Y., Makishima K., Iyomoto N., Hayashida K., Kohmura Y., Mushotzky R.F., Petre R., Serlemitsos P.J., Terashima Y. 1996, PASJ, 48, 237, 1996
Iwasawa K., Comastri A. 1998, MNRAS 297, 1219
Koyama K., Maeda Y., Sonobe T., Takeshima T., Tanaka Y., Yamauchi S. 1996, PASJ 48, 249
Kronberg P.P., Clarke J.N. 1978, ApJ 224, L51
Lutz D., Kunze D., Spoon H.W.W., Thornley M.D. 1998, A&A 333, L75
Makishima K., Tashiro M., Ebisawa K., Ezawa H., Fukazawa Y., Gunji S., Hirayama M., Idesawa E. et al. 1996, PASJ 48, 171
Malina R., Lampton M., Bowyer S. 1976, ApJ 209, 678
McKeith C.D., Greve A., Downes D., Prada F. 1995, A&A 293, 703
Moran E.C., Lehnert M.D. 1997, ApJ 478, 172

Muxlow T.W.B., Pedlar A., Wilkinson P.N., Axon D.J., Sanders E.M., de Bruyn A.G. 1994, MNRAS 266, 455
Ohashi T., Ebisawa K., Fukazawa Y., Hiyoshi K., Horii M., Ikebe Y., Ikeda H., Inoue H. et al. 1996, PASJ 48, 157
Okada K., Dotani T., Makishima K., Mitsuda K., Mihara T. 1998, PASJ 50, 25
Ptak A., Serlemitsos P., Yaqoob T., Mushotzky R., Tsuru T. 1997, AJ 113, 1286
Raymond J.C., Smith B.W. 1977, ApJS 35, 419
Sakano M., Koyama K., Tsuru T., Awaki H., Ueda Y., Takahashi T., Akiyama M., Ohta K., Yamada T. 1998, ApJ 505, 129
Schaaf R., Pietsch W., Biermann P.L., Kronberg P.P., Schmutzler T. 1989, ApJ 336, 722
Serlemitsos P.J., Jalota L., Soong Y., Kunieda H., Tawara Y., Tsusaka Y., Suzuki H., Sakima Y. et al. 1995, PASJ 47, 105
Strickland D.K., Ponman T.J., Stevens I.R. 1997, A&A 320, 378
Tanaka Y., Inoue H., Holt S.S. 1994, PASJ 46, L37
Terashima Y., Kunieda H., Misaka K., Mushotzky R.F., Ptak A.F., Reichert G.A. 1998a, ApJ 503, 212
Terashima Y., Kunieda H., Serlemitsos P.J., Ptak A. 1998b, in The Hot Universe, IAU symposium No. 188, ed K. Koyama, S. Kitamoto, M. Itoh (Kluwer Academic Publishers, Dordrecht) p444
Tsuru T. 1992, PhD Thesis, The University of Tokyo
Tsuru T.G., Awaki H., Koyama K., Ptak A. 1997, PASJ 49, 619
Tsuru T., Hayashi I., Awaki H., Koyama K., Fukazawa Y., Ishisaki Y., Iwasawa K., Ohashi T. et al. 1994, in New Horizon of X-Ray Astronomy, ed F. Makino, T. Ohashi (Universal Academy Press, Tokyo) p529
Tsuru T., Hayashi I., Awaki H., Koyama K., Fukazawa Y., Ishisaki Y., Iwasawa K., Ohashi T. et al. 1996, in X-ray Imaging and Spectroscopy of Cosmic Hot Plasmas, ed F. Makino, K. Mitsuda (Universal Academy Press, Tokyo) p157
Ueda Y., Takahashi T., Inoue H., Tsuru T., Sakano M., Ishisaki Y., Ogasaka Y., Makishima K. et al. 1998, Nature 391, 866
Watson M.G., Stanger V., Griffiths R.E. 1984, ApJ 286, 144
Yaqoob T., Warwick R.S., Makino F., Otani C., Sokoloski J.L., Bond I.A., Yamauchi M. 1993, MNRAS 262, 435